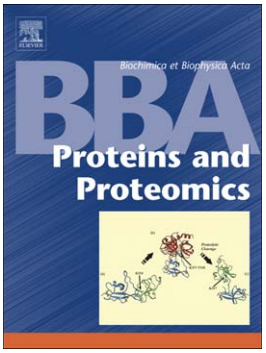

Connecting Imaging Mass Spectrometry and Magnetic Resonance Imaging-based Anatomical Atlases for Automated Anatomical Interpretation and Differential Analysis

Nico Verbeeck, Jeffrey M. Spraggins, Monika J.M. Murphy, Hui-dong Wang, Ariel Y. Deutch, Richard M. Caprioli, Raf Van de Plas

PII: S1570-9639(17)30040-7
DOI: doi:10.1016/j.bbapap.2017.02.016
Reference: BBAPAP 39904

To appear in: *BBA - Proteins and Proteomics*

Received date: 9 August 2016
Accepted date: 13 February 2017

Please cite this article as: Nico Verbeeck, Jeffrey M. Spraggins, Monika J.M. Murphy, Hui-dong Wang, Ariel Y. Deutch, Richard M. Caprioli, Raf Van de Plas, Connecting Imaging Mass Spectrometry and Magnetic Resonance Imaging-based Anatomical Atlases for Automated Anatomical Interpretation and Differential Analysis, *BBA - Proteins and Proteomics* (2017), doi:10.1016/j.bbapap.2017.02.016

Title:

Connecting Imaging Mass Spectrometry and Magnetic Resonance Imaging-based Anatomical Atlases for Automated Anatomical Interpretation and Differential Analysis.

Authors:

Nico Verbeeck[a] (n.verbeeck@tudelft.nl),

Jeffrey M. Spraggins[b,c,d] (jeff.spraggins@vanderbilt.edu),

Monika J.M. Murphy[e] (monika.murphy@vanderbilt.edu),

Hui-dong Wang[f] (huidong.wang@vanderbilt.edu),

Ariel Y. Deutch[e,f,g] (ariel.deutch@Vanderbilt.Edu),

Richard M. Caprioli[b,c,d,h] (richard.m.caprioli@vanderbilt.edu),

Raf Van de Plas[a,b,*] (raf.vandeplas@tudelft.nl)

[a] Delft Center for Systems and Control (DCSC), Delft University of Technology, Mekelweg 2, 2628 CD, Delft, the Netherlands

[b] Mass Spectrometry Research Center (MSRC), Vanderbilt University, 465 21st Ave. South, 9160 Medical Research Building III, Nashville, TN 37240, USA

[c] Department of Biochemistry, Vanderbilt University, 607 Light Hall, Nashville, TN 37205, USA

[d] Department of Chemistry, Vanderbilt University, 7330 Stevenson Center Station B 351822, Nashville, TN 37235, USA

[e] Program in Neuroscience, Vanderbilt University, U-1205 Medical Research Building III, 465 21st Ave. South, Nashville, TN 37232 USA

[f] Department of Psychiatry and Behavioral Sciences, Vanderbilt University Medical Center, 1211 Medical Center Dr. Nashville, TN 37232, USA

[g] Department of Pharmacology, Vanderbilt University, Nashville, 460B Preston Research Building, Nashville, TN 37232 , USA

[h] Department of Medicine, Vanderbilt University Medical Center, 1161 21st Ave. South, D-3100 Medical Center North, Nashville, TN 37232, USA

* Corresponding Author

Abstract (100 – 250 words)

Imaging mass spectrometry (IMS) is a molecular imaging technology that can measure thousands of biomolecules concurrently without prior tagging, making it particularly suitable for exploratory research. However, the data size often makes thorough extraction of relevant information impractical. To help guide and accelerate IMS data analysis, we recently developed a framework that integrates IMS measurements with anatomical atlases, opening up opportunities for anatomy-driven exploration of IMS data. One example is the automated anatomical interpretation of ion images, where empirically measured ion distributions are automatically decomposed into their underlying anatomical structures.

While offering significant potential, IMS-atlas integration has thus far been restricted to the Allen Mouse Brain Atlas (AMBA) and mouse brain samples. Here, we expand the applicability of this framework by extending towards new animal species and a new set of anatomical atlases retrieved from the Scalable Brain Atlas (SBA). Furthermore, as many SBA atlases are based on magnetic resonance imaging (MRI) data, a new registration pipeline was developed that enables direct non-rigid IMS-to-

MRI registration. These developments are demonstrated on protein-focused FTICR IMS measurements from coronal brain sections of a Parkinson's disease (PD) rat model, which are integrated with an MRI-based rat brain atlas from the SBA. The new rat-focused IMS-atlas integration is used to perform automated anatomical interpretation and to find differential ions between healthy and diseased tissue. IMS-atlas integration can serve as an important accelerator in IMS data exploration, and with these new developments it can now be applied to a wider variety of animal species and modalities.

Keywords:

imaging mass spectrometry, anatomical atlas, FTICR MS, MRI, rat brain

Abbreviations:

AMBA: Allen Mouse Brain Atlas

MRI: Magnetic resonance imaging

PD: Parkinson's disease

SBA: Scalable Brain Atlas

t-SNE: t-distributed stochastic neighbor embedding

FTICR: Fourier transform ion cyclotron

1. Introduction

Imaging Mass Spectrometry (IMS) is a powerful imaging technology that allows thousands of molecules to be detected throughout a tissue sample using a single experiment [1]. IMS enables direct comparison of proteomic, peptidomic, lipidomic, or metabolomic content between various tissue areas without the need for prior labelling of a target molecule [2,3]. These attributes have led to increased application of IMS in exploratory biomedical studies of a wide variety of diseases such as cancer [4–6], Parkinson's disease [7,8], Alzheimer's disease [7], macular degeneration [9], and diabetes [10,11]. Over the last decade, sample preparation and instrumental advances have greatly enhanced the depth of data that can be obtained by IMS [12], as well as the speed with which high-spatial-resolution experiments can be conducted [13]. These improvements, however, have also led to a large increase in the amount of data that is obtained by IMS experiments, with data sizes of individual experiments approaching 1 TB. In addition to being impractical and time consuming, manual interpretation often introduces human bias and drift into the exploration that ultimately leads to inexhaustive extraction of biologically relevant information. As a result, an increasing number of publications study multivariate data analysis techniques for extracting useful information from IMS measurements in an automated way. Examples of such techniques include principal component analysis (PCA) [14–16], probabilistic latent semantic analysis (pLSA) [17] and CUR matrix decomposition [18], t-distributed stochastic neighbor embedding (t-SNE) [19,20], and various clustering techniques [21,22], which all provide means of representing IMS data more concisely. While these techniques have been invaluable in advancing the ways in which IMS data are explored, they tend to operate in an IMS-centric fashion

and often do not take into account other (non-IMS) types of information that are known about the sample in question. One way of using such additional types of data in IMS analysis is by data-driven multi-modal fusion [23], where direct mining of relationships between IMS and its accompanying histology are used to predictively gain insights beyond the original IMS measurements. Another important source of external information, which is often used by researchers in the biological interpretation of IMS data, is anatomical knowledge on the tissue under examination. While such anatomical information is widely available in the form of anatomical atlases, its use is often limited by the fact that the (spatial and content-wise) link between ion images of interest and the anatomical atlas information usually needs to be established by manual interpretation. Such manual matching of molecular patterns to anatomical patterns is not only cumbersome and time consuming, but it is also prone to human bias and drift. In order to move the usage of anatomical information towards a more objective platform, we and other research groups [24,25] have recently proposed using spatial registration to establish a computational link between IMS data, obtained from mouse brain sections, and the Allen Mouse Brain Atlas (AMBA)[26].

Such a computer-traversable link between both data sources opens the door towards more advanced anatomy-based methods for IMS analysis. Examples of such methods were developed in our previous work [24], where we examined a number of different IMS analysis methods that leverage information from a registered anatomical atlas to guide a user towards relevant findings within a single IMS experiment. The simplest methods were correlation-based queries, in which the user specifies an anatomical structure of interest and the query returns ions relevant to

that structure in terms high correlation. Vice versa, when supplied with an ion image of interest, the query returns the anatomical structures that have the highest correlation with that ion image. However, in this publication we also demonstrated that correlation-based queries fall short in cases where there is "multi-membership", i.e. the ion of interest is present in multiple anatomical structures concurrently. Since multi-membership is a common occurrence in biological tissues, we introduced a novel method capable of handling it, termed 'automated anatomical interpretation'. The method makes it possible to have the spatial distributions in an ion image automatically interpreted as a combination of the anatomical structures provided by the atlas, similar to how a human investigator would deliver an interpretation. Since this method can automatically deliver anatomical annotations for hundreds of ion images in a time span much smaller than that needed for manually examination, it can serve as a powerful tool in the exploration of IMS data, particularly for the histological non-expert.

A second important advantage of linking IMS data to an anatomical atlas, is that it facilitates automated comparisons between multiple IMS experiments. Since spatial locations are generally not matched across experiments, i.e. the *x*th pixel in experiment A does not necessarily correspond to the *x*th pixel in dataset B, direct comparisons between IMS experiments are not straightforward. Mapping the individual data sets to a common anatomical atlas, however, can provide a reference plane in which spatial locations from different IMS experiments can be directly compared. This provides the opportunity to explicitly link these locations to the anatomical structures in which they reside. Carreira et al. [27] for example have used the AMBA reference plane in a cohort study on cortical spreading depression (CSD)

to investigate biomolecular changes at the anatomical level, while Škrášková et al. [28] have made use of this setup to accurately pinpoint the anatomic locations of lipids in SIMS data obtained from sagittal sections of mouse brain.

In this work, we extend the IMS-atlas integration beyond the mouse-focused studies that introduced it, and we expand the applicability of the automated anatomical interpretation framework [24] by means of the following developments:

(1) **New anatomical atlases, expanding the interpretation framework to non-mouse species.** Previous work on IMS-atlas integration has focused on mouse brain, using the AMBA as the source for curated information. To expand atlas-guided analysis to a broader set of animal species, we make the link to a new set of anatomical atlases available through the Scalable Brain Atlas (SBA) project [29] (http://scalablebrainatlas.incf.org). SBA is a web-based platform that provides access to a large collection of brain atlas templates for (currently) six different species, namely mouse, rat, marmoset, human, macaque, and opossum.

(2) **Direct non-rigid spatial registration of IMS to Magnetic Resonance Imaging (MRI).** The AMBA was defined on a basis of Nissl-stained microscopy images, allowing for straightforward registration to the histological images available in most state-of-the-art IMS experiments. Many atlases available through the SBA, however, are defined on the basis of MRI measurements rather than microscopy. To be able to establish a spatial link between IMS data and the SBA atlases, we developed a non-rigid registration pipeline that directly maps IMS data to an MRI reference image, without the need to go through histology. This is a non-trivial task as going

from the intact organ as observed by MRI to tissue sections introduces significant morphological distortions (e.g. tissue shrinkage and cutting artifacts).

(3) **Application of the IMS-atlas integration for finding biomolecular differences between IMS data sets, and providing automated anatomical interpretation for these differences.** While automated anatomical interpretation holds a lot of potential for exploring a single IMS experiment, here we demonstrate that an IMS-atlas framework can also be used to discover differentially expressed ions between IMS experiments. Additionally, these differential findings can be immediately and automatically tied to the relevant anatomical structures.

These innovations are demonstrated in a case study where protein-focused Fourier transform ion cyclotron (FTICR) IMS data from coronal brain sections of a Parkinson's Disease (PD) rat model is integrated with the Waxholm Space Sprague Dawley rat atlas of Papp et al. [30–32], available through the SBA.

2. Methods

This section describes the methodology used to integrate IMS data with an MRI-based rat brain atlas. We introduce the two data sources used in this work: (a) the protein-focused FTICR IMS data obtained from a coronal rat brain section as part of a case study on Parkinson's disease, and (b) the MRI-based anatomical rat atlas available through the SBA. Subsequently, details are provided on the

registration pipeline we developed to perform direct non-rigid registration between IMS and MRI data. This is followed by a more detailed look into the methods that use the IMS-atlas integration to analyze the IMS data.

2.1 IMS data source

The brain tissue sections of the case study were collected from a rat PD model, in which adult male Sprague-Dawley rats were deeply anesthetized with isoflurane, pretreated with desmethylimipramine (12.5 mg/kg, ip) and placed in a stereotaxic frame. After an incision of the dorsal surface of the skull and placement of a burr hole, animals were again injected with despramine. Ten minutes later 1.5 :L of 6-hydroxydopamine HBr (6-OHDA; 4.0:g/uL, free base) was unilaterally injected into the substantia nigra (AP: -5.4; L: 2.3; DV: -8.4) to selectively destroy nigrostriatal dopaminergic neurons. Although there is a crossed-nigrostriatal pathway, it is quite small, contributing well under 5% of the dopamine content to the contralateral striatum, and thus the contralateral striatum is usually referred to as the intact (control) side. All in-house animal experiments were performed with approval by the Vanderbilt Institutional Animal Care and Use Committee. Brain

tissue was harvested, snap frozen using liquid nitrogen, and stored at -80° C until use. Frozen brain tissue was sectioned in the coronal plane at 10 microns using a cryostat (-20° C, Leica CM3050S; Buffalo Grove, IL, USA) and thaw mounted onto conductive Indium-tin-oxide coated glass slides (Delta Technologies, Loveland, CO, USA). Samples were washed to remove interfering lipids and salts in sequential washes of 70% ethanol (30 seconds), 100% ethanol (30 seconds), Carnoy's fluid (6:3:1 ethanol:chloroform: acetic acid) (2 minutes), 100% ethanol (30 seconds), water with 0.2% TFA (30 seconds), and 100% ethanol (30 seconds)[33]. The MALDI matrix 2,5-dihydroxyacetphenone (DHA, Sigma-Aldrich Chemical CO., St. Louis, MO, USA) was applied using a TM Sprayer (HTX Technologies, Carrboro, NC, USA) and rehydrated as described previously [13,33,34]. MALDI IMS images were collected using a 15T Fourier transform ion cyclotron (FTICR) mass spectrometer (Bruker Daltonics, Billerica, MA, USA) with a spatial sampling resolution of 75 μm (laser spot size ~50 μm) and a mass resolving power of 50,000 (m/FWHM) at *m/z* 5,000. The molecular images focused on a *m/z* range of 1300 to 23,000 with a total of ~20,000 pixels. The instrument was tuned for protein imaging as described previously [13,34]. After

IMS acquisition, matrix was removed using 100% ethanol and the tissue was stained with hematoxylin and eosin (H&E stain) for histologic analysis. Data were imported into MATLAB 2015b (The Mathworks Inc., Natick, MA) for further data analysis, where they were normalized to TIC and peak picked, resulting in a total of 2611 peaks.

2.2 Anatomical atlas data source

The Scalable Brain Atlas (SBA) [29] is a web-based platform that provides access to a collection of brain atlas templates for (currently) six different species, namely mouse, rat, marmoset, human, macaque, and opossum. These templates are pooled together from brain atlases made publicly available by other research projects [30–32]. The main interface to the SBA is the atlas viewer, which allows exploration of the atlas in a 3-D interactive context. The SBA provides several atlas templates for rat brain. Since we are using brain tissue collected from Sprague-Dawley rats, we used the recently added Waxholm Space Sprague Dawley rat atlas by Papp et al. (2014) [30–32]. The term "Waxholm Space" refers to the reference space that has been proposed to unify different rodent brain

atlases [35], in an effort to facilitate comparison between them. The anatomical labels and regions in this atlas have been defined on the basis of T2*-weighed MRI and Diffusion Tensor Imaging (DTI) images. The brain was scanned on a 7T small animal MRI system (Magnex Scientific, Yarnton, Oxford, UK) while still in the cranium *ex vivo*, at a reported 39-µm spatial resolution. Further experimental details have been described previously [30–32]. Rather than using the down-sampled version available directly through the SBA, we employ the full original data available from the International Neuroinformatics Coordinating Facility (INCF) website [36], which is linked to through the SBA. We employ the full 3-D T2* weighted MRI volume of the rat brain (512x1024x512 voxels), and the registered 3-D annotated atlas volume, containing 79 different distinct anatomical structures (atlas v2 bundle). Figure 1 shows a 3-D rendering of the T2*-weighted MRI, and an example of a 2-D coronal section and its matching atlas labels. DTI volumes are also publicly available, but are not used in this work. The data were read into MATLAB 2016a (The Mathworks Inc., Natick, MA) using the 'Read Medical Data 3-D' package by Dirk Kroon, available through the MATLAB Central File Exchange [37].

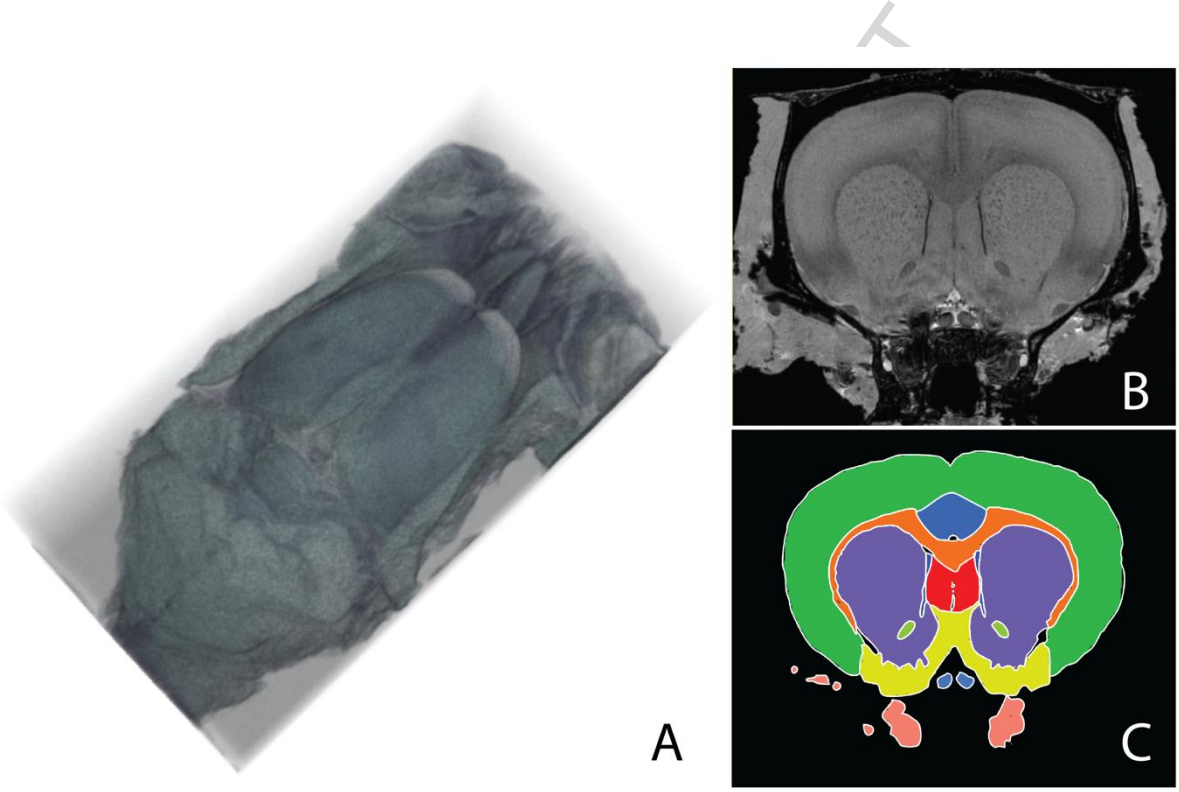

Figure 1. Waxholm Space Sprague Dawley rat atlas by Papp et al. [30–32] used as the anatomical data source. (A) 3-D rendering of the full T2* MRI rat brain data on which the anatomical annotations are based. The MRI was performed *ex vivo* while intact in the skull. (B) 2-D coronal section of the MRI data volume. (C) Anatomical labels for the coronal section shown in (B), as retrieved from the atlas. Panel (C) was generated using the SBA online viewer. The rat atlas in question contains a total of 79 anatomical labels.

2.3 IMS-atlas integration

To enable the integration of atlas information into the analysis of IMS data, the two data sources first need to be spatially mapped to each other. This allows measurements to describe the same reference space, making direct comparison possible. Beyond rigid spatial transformations such as rotations and translations, the use of non-rigid registration algorithms is often essential in the registration process between IMS and atlases [24,38]. These more advanced registration transformations provide the degrees of freedom needed to deal with cutting artifacts, biological variations, deformations such as shrinkage due to extraction and freezing of the brain, and other spatial perturbations. However, setting all those transformation variables to valid values also makes non-rigid registration a non-trivial process. Previous work on IMS-atlas integration (using the AMBA) facilitated this process by performing the non-rigid registration step within a single and common modality (e.g. optical microscopy) thereby reducing the complexity of the image-to-image matching task. Optical microscopy of stained tissue is readily available in most IMS experiments, and the AMBA itself is also defined on a basis of microscopy images, making microscopy a straightforward

intermediate for spatial registration between the two sides. In these cases, the overall registration pipeline consisted of (i) rigid registration of the IMS data to the experiment histology, (ii) rigid registration of the atlas labels to the atlas histology, and (iii) non-rigid registration of the experiment histology to the atlas histology. However, many of the atlases available through the SBA, including the Sprague Dawley rat atlas used here, are defined on the basis of MRI measurements, not microscopy images. As a result, the traditional microscopy-centric registration pipeline cannot be used. One could potentially register the experiment histology that accompanies many IMS experiments to MRI and thus, indirectly register IMS to MRI. However, in light of the added complexity that comes with registering different types of modalities to each other, it is deemed more prudent to avoid additional layers of indirection and instead perform the non-rigid registration directly between IMS and MRI. A further advantage of performing the registration directly between IMS and MRI is that IMS provides much richer biochemical information on a tissue section than microscopy does, providing more potentially corresponding image features to base a non-rigid registration to MRI on. A few studies have previously registered IMS to MRI [39–

41], however, it should be noted that these studies collected the different types of data from the same animal, making spatial registration less challenging than in a scenario with different animals as is the case here (IMS animal vs. atlas animal). In those cases, manual alignment and basic rigid registration algorithms could be used for the IMS-to-MRI registration, approaches that are generally less suited to deal with the natural biological variation that occurs between different animals. To accommodate for these biological perturbations as well, we establish a more elaborate non-rigid registration approach.

2.3.1 Dimensionality reduction

A practical issue with using IMS data to perform registration is that these data sets consist of hundreds to thousands of ion images, whereas, in general, registration algorithms expect a single image as an input for the registration process. Rather than (manually) searching among the many ion images available for a single ion image that can be used to perform the registration, a faster and more robust approach is to maximally bring together the information of all ion images into a limited set of consensus images. This can be accomplished by

using dimensionality reduction techniques to extract the most important trends from the data and encode them as lower-dimensional 2-D patterns. From this limited set of consensus images, we can then select the image that is best suited for the registration with MRI. Our approach was to create such consensus images using principal component analysis (PCA), an analysis technique that has been widely applied in IMS research [14–16]. A similar concept has been employed in IMS-histology registration by Abdelmoula et al.[38], who used another dimensionality reduction technique, t-distributed stochastic neighbor embedding (t-SNE) [20], to create a single composite image of the IMS data. Here, PCA is used to reduce the dimensionality of the IMS data set, i.e. describe the data set using a smaller number of variables while still retaining as much of the original variation as possible. The new variables, called the principal components (PCs), are defined such that they give the orthonormal directions of maximal variation in the data set, ensuring that the PCs are not correlated to each other. This forms a new orthonormal basis, where the first PC basis vector lies along the direction of the largest variance in the dataset. The second PC basis vector is orthogonal to the first and lies along the direction of second largest variance, etc. Using this

approach, the majority of variation in many real-life datasets, including IMS data, can be captured by a number of PCs that is much smaller than the original number of variables. In IMS research, the loadings of the PCs are taken to be on the spectral side, and represent sets of correlating ions, while the scores of the PCs represent the spatial expression of the PC in the tissue (or vice versa depending on how the original matrix is organized). These spatial expressions can be visualized as images, and it is these PC images that were used in the registration process.

2.3.2 IMS-MRI registration

With these reduced consensus images, the registration between the IMS data and the MRI data (and implicitly the atlas) can now be performed as follows:

(i) *Selection of the relevant atlas depth.* We perform manual selection of the coronal atlas section (and thus MRI depth) that exhibits the best structural match to the coronal brain section used in the IMS experiment. Since the MRI measurements are performed on an intact brain still inside the skull, we mask out

any areas outside the brain that are not measured in the IMS experiment, making use of the standard MATLAB functions *bwselect* and *imfill*.

(ii) *Reduction of the total number of molecular images from IMS to a set of consensus PC expression images.* We perform PCA on the IMS data, and manually select the PC whose spatial expression best matches that observed in the MRI image selected from the atlas.

(iii) *Calculate a non-rigid registration transformation between the PC expression image on the IMS-side and the MRI image on the atlas-side.* We use the Medical Image Registration Toolbox (MIRT) by Myronenko [42,43] to calculate a free form deformation (FFD) model-based non-rigid transformation between the two images. The squared correlation coefficient is used as similarity measure, analogous to the non-rigid registration step we established in Verbeeck et al. [24].

(iv) *Registration of ion images to anatomical atlas labels.* Given that the consensus PC expression image describes the same spatial coordinate space as the original ion images, and the anatomical annotations of the atlas are defined in the same reference space as the MRI measurements, the non-rigid

transformation established in the previous step implicitly registers the IMS measurements to the atlas and its annotations.

2.4 Atlas-guided differential analysis

Once registration is complete, each pixel in the IMS data set is spatially linked to a particular location in the atlas. We can now use this link to guide the analysis of our IMS data using anatomical annotations. In our case study specifically, we are interested in the biomolecular changes between the dopamine depleted hemisphere and the healthy hemisphere, and the anatomical regions of the brain in which these changes occur. In order to find such differences, we first divide the registered IMS data into two separate data sets, separating mass spectra located in the healthy hemisphere from mass spectra located in the dopamine depleted hemisphere. Using the IMS-atlas link, we connect each spectrum to the anatomical regions their acquisition location overlaps with, and we do this for both hemispheres/data sets. For each anatomical region individually, we can then compare the biomolecular content of that anatomical structure between the two

hemispheres. The Wilcoxon rank-sum test, a standard non-parametric statistical test, is used to automatically find ions that are expressed differentially between the two hemispheres per anatomical zone. This allows us to univariately compare the expression of each ion over the whole anatomical region in question between the healthy and diseased hemisphere. While this univariate approach is a relative simple approach, and can present potential multiple testing challenges, it serves as a useful and fast manner to obtain quick insight into which ions and anatomical structures exhibit interesting differential behavior between two IMS data sets. The overall goal is not to obtain a minimum of false positives or establish a notion of statistical significance, but rather to provide a fast tool to reduce the complexity of differential comparisons between IMS experiments and to guide the user towards potential ions of interest.

2.5 Automated anatomical interpretation

Besides the atlas-guided data exploration that the IMS-atlas link enables, we can also directly apply automated anatomical interpretation on the basis of this new atlas. Automated anatomical interpretation is a computational technique

previously introduced for the AMBA [26], which automatically interprets the spatial distributions observed in any registered ion image as a combination of the anatomical structures described in the atlas. Briefly, the algorithm approximates a provided ion image as a sum of products, where each product multiplies a pattern from the set of all the anatomical structure patterns available in the atlas with its contributing factor. The model aims to find the optimal approximation of the original ion image by solving this approximation as a multivariate optimization problem, which searches for the "best" combination of anatomical structure contributions to explain what is observed in the ion image. The optimization problem is solved using CVX, a MATLAB-based modeling package for specifying and solving convex programs [44,45]. An interesting aspect of this approach is that the weight of each anatomical structure tends to be proportional to the ion intensity in that anatomical structure, providing an inherent notion of importance to each anatomical structure involved. Furthermore, this anatomical interpretation is fully automated, and can easily be performed in parallel for each of the hundreds to thousands of ion images in an

IMS dataset. We refer to the aforementioned publication for full details on this method.

3. Results & discussion

This section first gives an overview of the spatial registration results, highlighting the direct non-rigid registration between the empirically acquired IMS data and the MRI data from the rat brain atlas. Once registration between the data sources is attained, we demonstrate the application of this new IMS-atlas combination towards the discovery at the anatomical level of ions that are differential between two IMS data sets (left versus right hemisphere). Finally, we use the atlas data to perform automated anatomical interpretation of ion images acquired in rat brain.

3.1 Spatial registration of data sources

3.1.1 Dimensionality reduction

To relate the IMS and atlas data to each other, we first need to bring both data sources into a common spatial coordinate system. This is accomplished by spatially registering the two sources to each other. Since the registration

algorithm expects each of the data sources to be represented by a single image, which can then be spatially mapped to each other, the natively high-dimensional IMS data is transformed into a lower-dimensional representation that tries to maintain as much relevant information from the original IMS measurements as possible. In this case study, we applied standard PCA [46] as a means of dimensionality reduction, followed by manual selection among PCs to come to a single consensus image that yields the most relation to the corresponding MRI image from the atlas. Figure 2.A shows the spatial expression patterns of the first six PCs obtained from the IMS data set by applying PCA. The next step is to select the spatial expression image that best matches the MRI reference image that needs to be registered to (shown on the bottom right in Figure 2, cropped and with the rat skull removed). Of the six PCA-derived image patterns, PC5 exhibits a spatial distribution that closely matches that of the MRI image. This becomes particularly apparent when the PC expression image is transformed to a greyscale map and the colored background is removed (see left image in Figure 2.B). Since this PC expression image shares the same spatial coordinate system as the ion images in the data set, it can now be used directly as the image

representative of the IMS-side and as input to the non-rigid registration algorithm.

An interesting observation regarding the motivation for a dimensionality reduction approach is that there is no individual ion image in this IMS dataset that exhibits the same spatial expression as seen in PC5 or that matches the MRI image more closely. The pattern observed in PC5 is a combination of multiple distinct ion images, collecting into one the spatial distribution that in the raw data set lies spread across multiple ion species. This seems to indicate that unless you have a particular ion image that correlates well with the corresponding MRI image, it is beneficial to employ some form of dimensionality reduction technique to generate a consensus image that reports information from across multiple ion species.

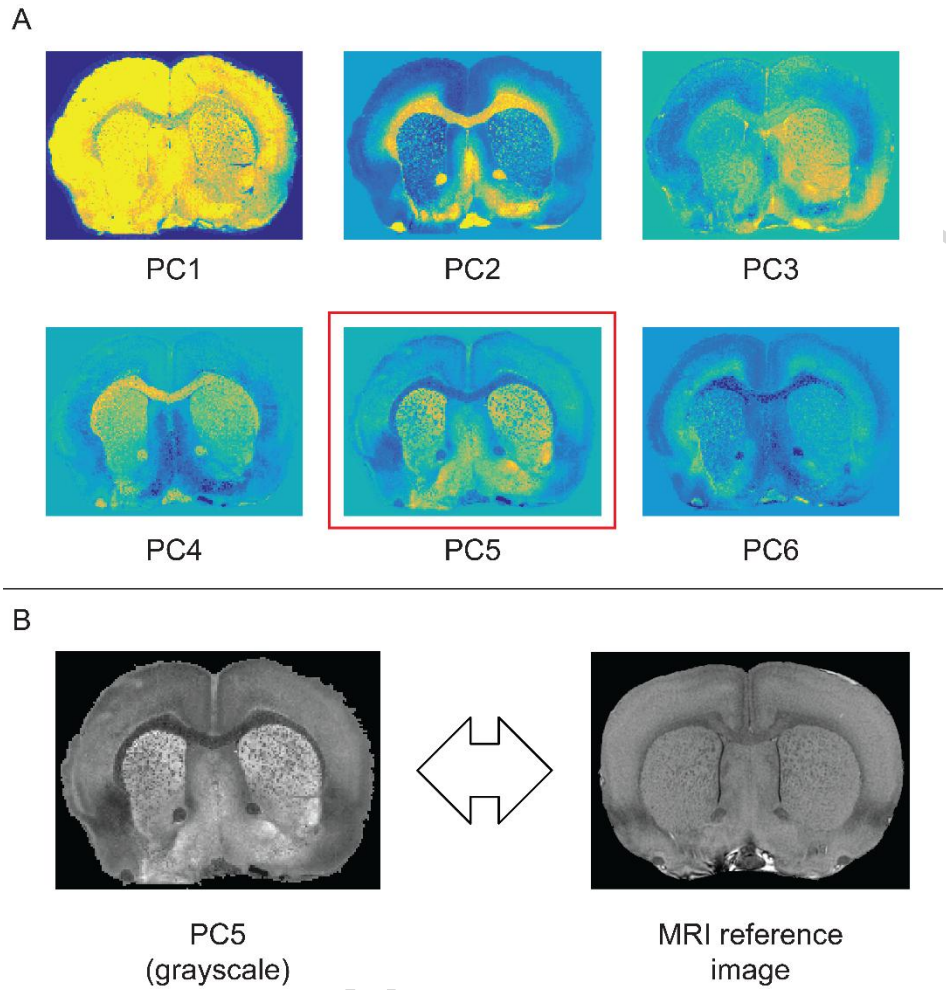

Figure 2. (A) The spatial expression patterns of the first six principal components (PCs) obtained from the IMS data set by applying PCA. PC5 exhibits a spatial distribution that closely matches that of the MRI reference image. (B) The expression image of PC5 (left) is transformed to a grayscale map and the colored background is removed. This image can be used directly as an input for the non-rigid registration with the MRI reference image (right).

3.1.2 Non-rigid registration

The IMS consensus image (5th PC image) and the MRI reference image are spatially registered to each other using a non-rigid registration algorithm, provided by the MIRT toolbox by Myronenko [42,43], making use of a free form deformation (FFD) model and the squared correlation coefficient as the similarity measure. Since we use a FFD model as the basis for the non-rigid transformation, the registration process provides as its output a mesh of control points that maps spatial locations in the IMS consensus image to spatial locations in the MRI reference image. Figure 3.A summarizes these results, showing the original IMS consensus image (a), the original MRI reference image (d), the mesh of control points determining the registration (b), and the resulting registered version of the IMS consensus image (c). Figure 3.B furthermore shows an overlay of the registered IMS consensus image and the MRI reference image (e), showing good agreement between the two images. By using the FFD model, its transformation mesh ensures that neighboring pixels in the IMS data remain neighbors after the registration process, and prevents excessive warping of the original data. Once a non-rigid registration and transformation mesh has been established, each pixel

location in the IMS data is linked to a pixel location in the MRI image. As the anatomical labels from the atlas are registered directly to the MRI data, this also means that each spatial location in the IMS data is now implicitly registered to the atlas content and thus annotated with anatomical labels. In effect, the registration of both data sources to each other allows data from the atlas space to be directly projected onto the IMS space, and vice versa. Figure 3.B shows an example of an ion image projected onto the reference space (f). The anatomical information from the atlas can now be directly incorporated into the analysis of the IMS data.

These results demonstrate the feasibility of direct non-rigid registration between IMS data and MRI data. On the one hand, this task is helped by the richness of the biochemical data acquired by IMS. The richer the information that is collected by a modality, the higher the chance is that there is an overlap with the patterns or features acquired by the other modality, and the more material there is available to establish a reliable registration transformation with. On the other hand, it remains a challenge on how to effectively bring the bulk of that rich

information together into a single image, as is expected by most registration algorithms. We and others have been using dimensionality reduction approaches to accomplish this, but it is clear this area still leaves room for more advanced approaches to be developed.

While our proof-of-concept implementation of this methodology demonstrates its feasibility in rat brain, there are no inherent ties to a particular sample type and the approach should be applicable in any scenario where IMS-MRI registration is pursued. This opens the path towards integration of IMS data with any MRI-based atlas, whether it is for another animal species within the SBA, or to one of a multitude of other MRI-based atlases available online [47]. It should also be noted that the registration pipeline that is described here, is performed between data from different animals. It is expected to be equally applicable in the relatively less complex case where IMS and MRI data are collected from the same animal.

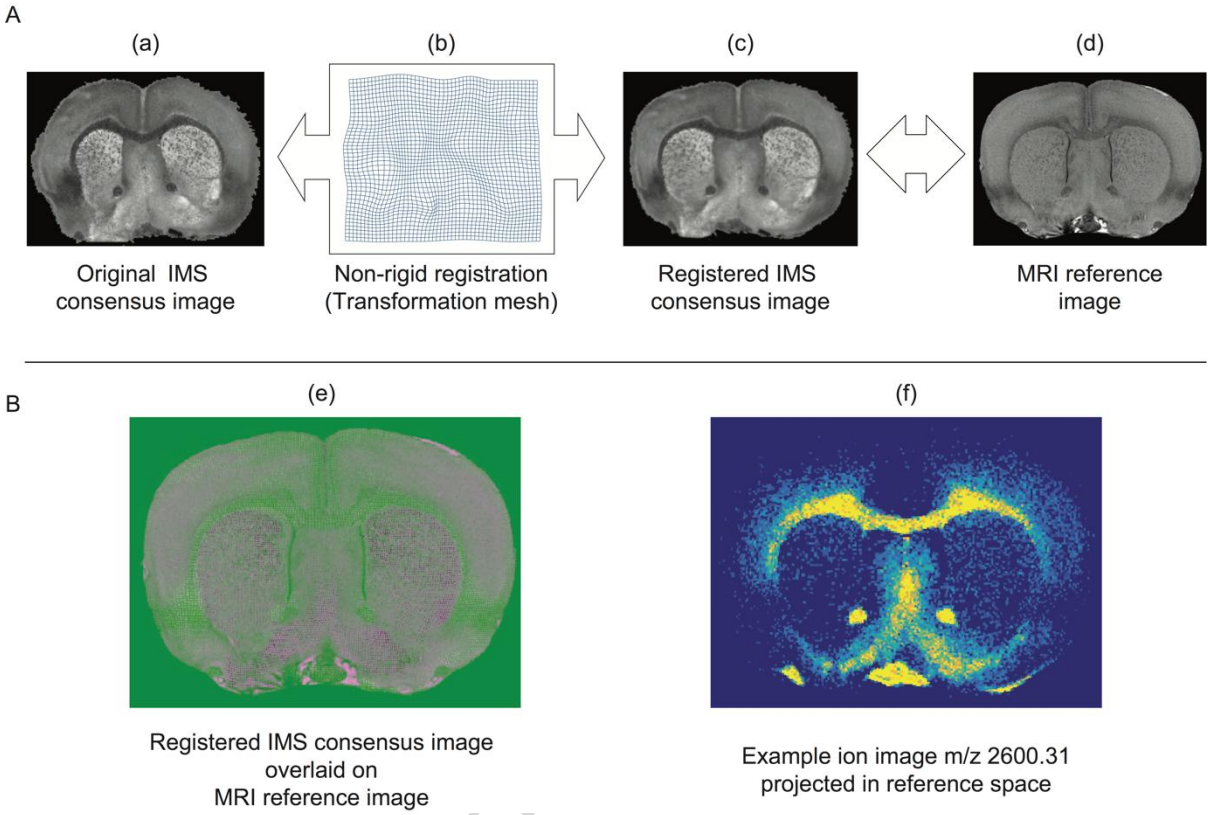

Figure 3. (A) Non-rigid registration of the original IMS consensus image (a) to the MRI reference image (d). The mesh of control points (b) establishes the non-rigid registration between (a) and (d), resulting in the registered IMS consensus image (c). (B)(e) Overlay of the registered IMS consensus image (green) on the MRI reference image (pink) showing satisfactory registration results. Once established, the non-rigid registration allows projection of data from one data source to the other, here exemplified by an ion image projected onto the reference space.

3.2 Atlas-guided differential analysis

This section demonstrates how the rat-focused IMS-atlas framework can be used to retrieve, per anatomical structure, differentially expressed ions between the control and diseased hemispheres in our rat PD model. As shown in Figure 4.A, the IMS measurements are divided into two parts: mass spectra belonging to the dopamine depleted hemisphere (left) versus mass spectra belonging to the control hemisphere (right). Using the labels directly provided by the registered atlas, we can now group together in each hemisphere the spectra/pixels that belong to a particular anatomical structure, which allows us to compare the biochemical content per anatomical structure between the two hemispheres. This enables questions such as "which protein ions are up/down-regulated in the cortex between the control and diseased hemisphere?" to be asked. The Wilcoxon rank-sum test is used per ion species to determine whether that ion is differentially expressed for a particular anatomical structure using the standard 0.05 significance level in MATLAB. For our example, we are mostly interested in large differences, and therefore further impose that the ion must be at least two-fold up/down-regulated over the anatomical structure, i.e. the median expression

of the ion in the anatomical region must be at least two times higher/lower between the hemispheres. By collecting the number of differentially expressed ions per anatomical structure, we can create a spatial heatmap as shown in Fig. 4.B, panel (a). This sort of visualization gives an immediate overview of where in the tissue, and where in terms of anatomy the largest biomolecular differences occur for this data set. The color scale of the spatial heatmap ranges from dark red to bright yellow, where dark red means relatively few biochemical changes and bright yellow means a relative large number of biochemical changes. Panel (c) of Figure 4 furthermore summarizes, for specific anatomical structures, which ions are up and down regulated at least two-fold between disease and control, where positive peaks indicate up-regulation in the disease and negative peaks indicate down-regulation in the disease compared to the control. The chemical changes heatmap in panel (a) indicates that the largest number of differential ions can be found in the cortex (17 differential ions) and the striatum (20 differential ions), while only a limited number of changes occurs in the septal region (3 differential ions). The relatively large number of differential ions detected in the cortex is particularly interesting because nigral dopamine neurons

innervate only very small areas of the rat cortex (at the levels analyzed, portions of the supragenual cingulate and piriform cortices. Although these changes need to be verified with additional replicates and further work is needed to identify the up/down-regulated biomolecules of the cortex, these observations clearly demonstrate the unique capabilities of imaging MS to provide spatially specific molecular measurements and the necessity to provide anatomical context to these rich data sets. Moreover, the current data suggest that the method may be a very useful postmortem adjunct to network connectivity studies of Parkinson's Disease, one that provides chemical specificity in contrast to the varied and poorly understood signals used for connectivity analyses. In Figure 5 we show some example images of up and down-regulated ions in the cerebral cortex and striatum. These ion images show the clear impact of the dopamine depletion on the expression of protein ions in the left and right hemisphere of the rat brain tissue, and show that this impact can be seen in various anatomical structures.

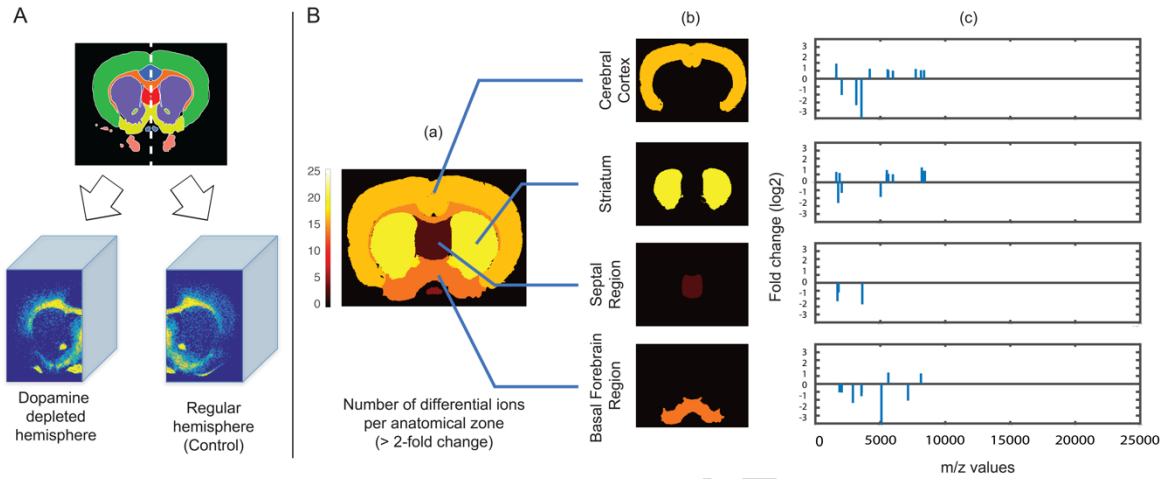

Figure 4. (A) The IMS dataset is split into two parts, namely pixels belonging to the dopamine depleted hemisphere and pixels belonging to the control hemisphere. (B) After the differential analysis, a spatial heatmap (a) can be created, which gives an overview of the number of differential ions per anatomical zone. For our analysis, we are interested in ions that are up/down-regulated at least two-fold. Dark red means relatively few biochemical changes, while bright yellow means a relatively high number of changes. The results for individual anatomical structures are shown in (b) and (c), where (c) plots the ions that are up /down regulated at least two-fold between disease and control (positive peaks = up-regulation in the disease, negative peaks = down-regulation in the disease).

We do note that the granularity of the annotations provided by the rat atlas is relatively coarse. The anatomical annotations provided by the rat brain atlas from the SBA we used here, amounts to only 79 labels. By comparison, the previously used AMBA, which is one of the richer anatomical atlases available online, has over 800 distinct anatomical labels. The smaller number of rat brain labels leads to larger and less specific anatomical structures than those in the AMBA. However, the automated labelling provided by the IMS-atlas framework still allows for a much more targeted differential analysis than simply searching for ions that are differently expresses between the left and right hemisphere as a whole. Furthermore, the implicit availability of anatomical annotations can help guide the user towards specific biomolecular changes in an anatomical structure of interest, such as those in Figure 5. Once targets of interest have been identified, these can still be refined manually to smaller anatomical sub-regions.

While we use a univariate approach here, targeting differences in individual anatomical structures, it is apparent that the differential expression of many ions is not restricted to a single anatomical structure, but rather involves several

anatomical structures. For example, ion *m/z* 5549.85 in Figure 5 is differentially expressed in both the striatum and the cerebral cortex, and is therefore retrieved for both structures separately, but no automatic connection is made between the two. Such multi-membership cases cannot be described using univariate measures alone, and require the construction of a multivariate model, as demonstrated in the next section.

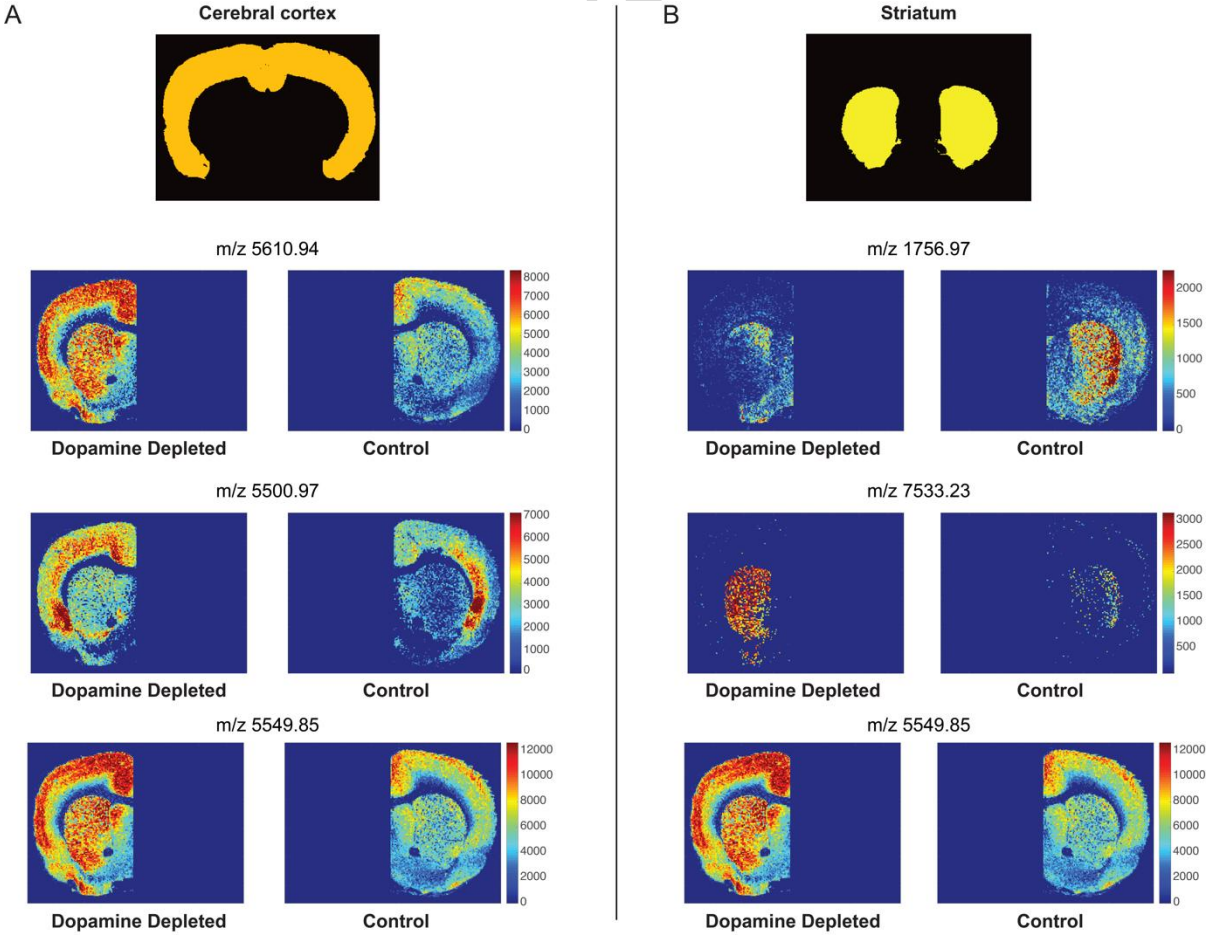

Figure 5. Several example ions that are differentially expressed between the dopamine depleted and control hemisphere in the cerebral cortex (A) and the

striatum (B). Ion *m/z* 5549.85 (bottom) is an example of an ion that is differentially expressed in both the striatum and the cerebral cortex, and is retrieved separately for each structure.

3.3 Automated Anatomical Interpretation

In previous work on the integration of IMS data with the AMBA [24], we introduced automated anatomical interpretation, a method to deconstruct the spatial distribution of an ion in terms of multiple anatomical structures. Here, we demonstrate that this method can be applied to IMS measurements from rat as well by using the new rat-focused atlas as the source of anatomical information. The automated anatomical interpretation algorithm takes an ion image as an input and aims to approximate it using a linear combination of the anatomical structure patterns that are provided by the atlas. The convex optimization approach that is used, ensures that the optimal linear combination, i.e. the combination that provides the closest approximation to the measured ion image, is retrieved. In Figure 6, we show an example of the automated anatomical interpretation applied to an individual ion image (left hemisphere) at *m/z*

5,549.85. The original ion image is shown to the left, while the closest approximation using anatomical regions, delivered by the algorithm, is shown to the right. The figure furthermore shows a breakdown of the most important anatomical structures involved in the approximation, and their relative contribution weights. The experiment shows good matching between the original ion image and the anatomical interpretation, which also further confirms the successful registration between IMS and MRI data. The anatomical breakdown immediately gives an overview of the anatomical regions involved in the expression of the ion image, and the algorithm correctly identifies the large role that the cerebral cortex, cingulate cortex, and striatum play in the expression of the ion (high weights in the anatomical interpretation). Furthermore, it recognizes the lower intensity in the corpus callosum by giving this structure a negative weight, indicating that the ion has a low relative abundance there. Overall, the automated anatomical breakdown is similar to how a human investigator would explore the image pattern, given the anatomical structures provided by the atlas. However, as we noted previously in section 3.2, the rat brain atlas that we use here has relatively coarse labels compared to for example the AMBA. As the

anatomical interpretation is based directly on the labels provided by the anatomical atlas, the anatomical breakdown can only be as detailed as the atlas allows. For example, the area indicated in Fig. 6 is actually a subarea of the cortex, the piriform area, which has a separate label in the AMBA, but not in the rat brain atlas. The ion intensity in this sub-area seems to be different from the rest of the cortex, but the algorithm does not have a separate structure to express this difference with, resulting in suboptimal interpretation. It is clear that the automated anatomical interpretation algorithm cannot go beyond the patterns provided to it by the atlas that the user supplies. However, even if the atlas is not as granular as one would desire, the algorithm will always give the most granular interpretation that the atlas allows, providing at least some guidance along a particular family of anatomical regions. Additionally, it should be noted that the method can automatically do the anatomical interpretation for each of hundreds to thousands of ion images in an IMS dataset, without requiring any further user interaction. The method thus provides a great tool to aid in the exploration of IMS data, by integrating a body of anatomical research

directly into the IMS data analysis, and directly tying ion expressions to anatomical information, bridging the gap between measurement and biology.

Incorporating into the analysis the notion of multi-membership of an ion to multiple anatomical zones, opens the way towards a deeper and more specific differential analysis than the univariate analysis described in section 3.2. The multi-membership model developed in Verbeeck et al. [24], allows us to search for ions that are, for example, exclusively differentially expressed in the cortex and not in other structures, or are expressed in both the cortex and the striatum etc. The translation of ion distributions to anatomical terms can be used in the analysis of data within the same tissue section, or sections collected in the same cutting plane, but it can also be used to compare expressions in the same anatomical structure at different depths in the brain. Moreover, the adoption of the new non-rigid registration pipeline enables the integration with atlases of different species in the SBA. Using the anatomical labels in the atlases can facilitate and automate the comparison of the biochemical content in anatomical zones across different animal species.

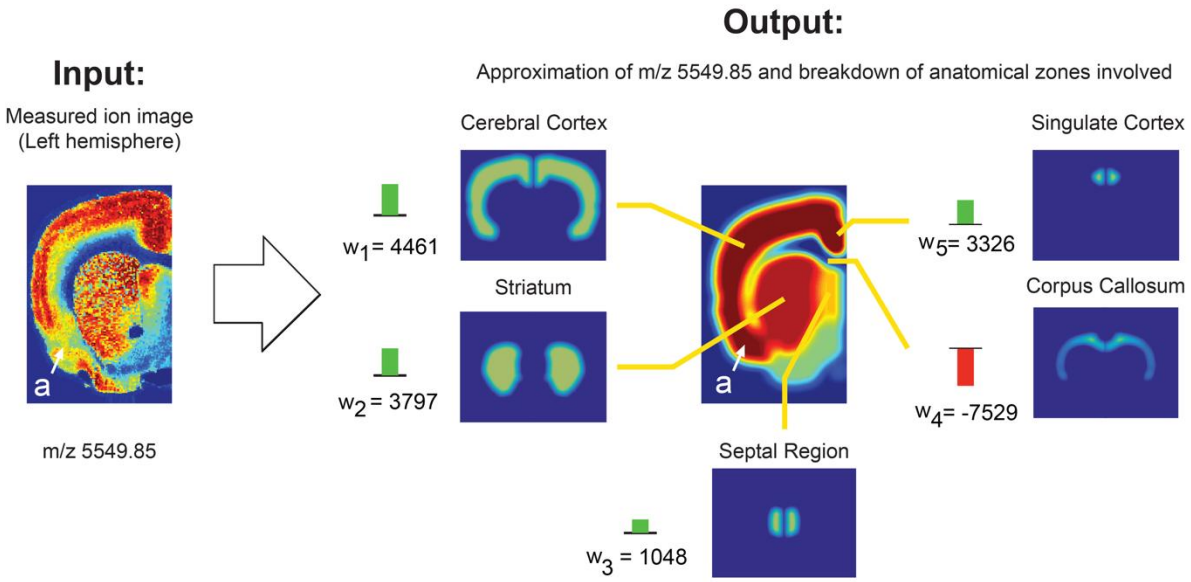

Figure 6. Example of automated anatomical interpretation. The automated anatomical interpretation algorithm takes an ion image, *m/z* 5549.85, as an input (left), and delivers the closest approximation (right, center) as an output, using the anatomical regions provided by the atlas. The algorithm also provides a breakdown of the most important anatomical structures involved in the approximation (outer ring), and their relative contribution weights. It correctly identifies the strong involvement of the cerebral cortex, cingulate cortex, and the striatum in the expression of the ion image, attributing high contribution weights to these structures. The corpus callosum is given a negative weight, which indicates a low relative expression in that anatomical area. Overall, the resulting

anatomical analysis shows a close match with the ion expression observed in the original ion image.

4. Conclusions

Previously, IMS-atlas integration and the applications it enables, e.g. automated anatomical interpretation, were restricted to mouse and using the Allen Mouse Brain Atlas. Here, we presented several new developments aimed at expanding the applicability of IMS-atlas integration to a wider array of atlases and animal models. A new set of anatomical atlases, available through the Scalable Brain Atlas project, were highlighted and connection to them was demonstrated. As many of the atlases in the SBA are MRI-based, we developed a novel registration pipeline that enables direct non-rigid IMS-to-MRI registration, which we demonstrate on protein-focused FTICR IMS data collected in a rat PD model, and an MRI-based rat brain atlas. We showed that PCA can be successfully used to extract consensus images from the rich IMS data, which can then be registered to the MRI data, providing accurate registration results. This same methodology should be applicable to any scenario where IMS-MRI integration is pursued and

is not restricted to integration with the SBA atlases alone. There still remain several open areas for improvement in the current IMS-atlas registration pipeline. The first is the selection of consensus images used in the registration. This image is currently selected manually from the reduced set of consensus images, however a computational approach could automate and optimize this step, potentially further improving registration results. A second area of improvement is the selection of the best matching tissue image in the atlas. Currently this step is performed manually, and towards the future this would preferentially be performed in an automated way.

We demonstrated the utility of the IMS-atlas framework by applying it to retrieve ions that differentiate, in an automated way, healthy rat brain tissue from diseased rat brain tissue per anatomical region. The IMS-atlas integration can help streamline IMS data exploration by providing anatomy-based tools, such as the presented change heatmap, which can guide the user towards anatomical regions with substantial biochemical change.

The quality of these analyses is tied directly to the quality of the labeling in the atlas. Despite the labeling of the rat brain atlas being relatively coarse compared

to that of the AMBA, a wide number of anatomical region-specific differential ions could be retrieved using this automated methodology. Moreover, the used rat brain atlas is still actively being updated, and as the detail of the annotations in the atlas improves, so will the quality of the automated IMS annotations.

We furthermore used the rat brain atlas to perform automated anatomical interpretation for the first time in a rat case study. This method translates the spatial distributions observed in ion images into anatomical terms, providing weights that exemplify how strongly an ion is expressed in each of the anatomical structures involved. The automated anatomical breakdown procured in this way can be obtained in an automated fashion, which allows it to avoid the laborious task of manually examining hundreds of ion images. It can side-step issues of drift and bias that sometimes play a role in human interpretation of image patterns.

In summary, IMS-atlas integration can serve an important role in further automating and streamlining IMS data exploration and analysis. The addition of

new atlases and a more advanced registration pipeline opens the way to adapt this approach for a growing number of animal species and modalities.

5. Acknowledgements

We acknowledge Andriy Myronenko for his work on the MIRT toolbox and making this tool available to us. This work was supported by the U.S. National Institutes of Health Grants 5R01 GM058008-16, NIH/MH-077298, and NIH/NIGMS 2P41 GM103391-06 and the National Institutes of Health Shared Instrumentation Grant Program 1S10OD012359-01. The content is solely the responsibility of the authors and does not necessarily represent the official views of NIGMS, NIMH, or the NIH.

6. References

[1] R.M. Caprioli, T.B. Farmer, J. Gile, Molecular Imaging of Biological Samples: Localization of Peptides and Proteins Using MALDI-TOF MS, Anal. Chem. 69 (1997) 4751–4760. doi:10.1021/ac970888i.

[2] L.A. McDonnell, R.M.A. Heeren, Imaging Mass Spectrometry., Mass Spectrom. Rev. 26 (2007) 606–43. doi:10.1002/mas.20124.

[3] M. Stoeckli, P. Chaurand, D.E. Hallahan, R.M. Caprioli, Imaging mass spectrometry: a new technology for the analysis of protein expression in mammalian tissues., Nat. Med. 7 (2001) 493–6. doi:10.1038/86573.

[4] C. Schöne, H. Höfler, A. Walch, MALDI imaging mass spectrometry in cancer research: Combining proteomic profiling and histological evaluation, Clin. Biochem. 46 (2013) 539–545. doi:10.1016/j.clinbiochem.2013.01.018.

[5] K.A. Veselkov, R. Mirnezami, N. Strittmatter, R.D. Goldin, J. Kinross, A.V.M. Speller, T. Abramov, E.A. Jones, A. Darzi, E. Holmes, J.K. Nicholson, Z. Takats, Chemo-informatic strategy for imaging mass spectrometry-based hyperspectral profiling of lipid signatures in colorectal cancer., Proc. Natl. Acad. Sci. U. S. A. 111 (2014) 1216–21. doi:10.1073/pnas.1310524111.

[6] K. Schwamborn, R.M. Caprioli, Molecular imaging by mass spectrometry--looking beyond classical histology., Nat. Rev. Cancer. 10 (2010) 639–46. doi:10.1038/nrc2917.

[7] J. Hanrieder, N.T.N. Phan, M.E. Kurczy, A.G. Ewing, Imaging Mass Spectrometry in Neuroscience, ACS Chem. Neurosci. 4 (2013) 666–79. http://pubs.acs.org/doi/abs/10.1021/cn400053c.

[8] J. Pierson, J.L. Norris, H.R. Aerni, P. Svenningsson, R.M. Caprioli, P.E. Andren, Molecular profiling of experimental Parkinson's disease: direct analysis of peptides and proteins on brain tissue sections by MALDI mass spectrometry, J Proteome.Res. 3 (2004) 289–295.

[9] D.M.G. Anderson, Z. Ablonczy, Y. Koutalos, J. Spraggins, R.K. Crouch, R.M. Caprioli, K.L. Schey, High resolution MALDI imaging mass spectrometry of retinal tissue lipids., J. Am. Soc. Mass Spectrom. 25 (2014) 1394–403. doi:10.1007/s13361-014-0883-2.

[10] S.M. Green-Mitchell, L.H. Cazares, O.J. Semmes, J.L. Nadler, J.O. Nyalwidhe, On-tissue identification of insulin: in situ reduction coupled with mass spectrometry imaging., Proteomics. Clin. Appl. 5 (2011) 448–53.

doi:10.1002/prca.201000152.

[11] K.J. Grove, P.A. Voziyan, J.M. Spraggins, S. Wang, P. Paueksakon, R.C. Harris, B.G. Hudson, R.M. Caprioli, Diabetic nephropathy induces alterations in the glomerular and tubule lipid profiles, J. Lipid Res. 55 (2014) 1375–1385. doi:10.1194/jlr.M049189.

[12] A. Römpp, B. Spengler, Mass spectrometry imaging with high resolution in mass and space., Histochem. Cell Biol. 139 (2013) 759–83. doi:10.1007/s00418-013-1097-6.

[13] J.M. Spraggins, D.G. Rizzo, J.L. Moore, M.J. Noto, E.P. Skaar, R.M. Caprioli, Next-generation technologies for spatial proteomics: Integrating ultra-high speed MALDI-TOF and high mass resolution MALDI FTICR imaging mass spectrometry for protein analysis, Proteomics. 16 (2016) 1678–1689. doi:10.1002/pmic.201600003.

[14] G. McCombie, D. Staab, M. Stoeckli, R. Knochenmuss, Spatial and Spectral Correlations in MALDI Mass Spectrometry Images by Clustering and Multivariate Analysis, Anal. Chem. 77 (2005) 6118–6124. http://pubs.acs.org/doi/abs/10.1021/ac051081q.

[15] R. Van de Plas, F. Ojeda, M. Dewil, L. Van Den Bosch, B. De Moor, E. Waelkens, Prospective Exploration of Biochemical Tissue Composition via Imaging Mass Spectrometry Guided by Principal Component Analysis, in: Pac. Symp. Biocomput., Maui, Hawaii, Singapore, 2007: pp. 458–69. http://europepmc.org/abstract/med/17990510 (accessed September 25, 2015).

[16] E.R. Muir, I.J. Ndiour, N.A. LeGoasduff, R.A. Moffitt, Y. Liu, M.C. Sullards, A.H. Merrill, Y. Chen, M.D. Wang, Multivariate Analysis of Imaging Mass Spectrometry Data, in: 2007 IEEE 7th Int. Symp. Bioinforma. Bioeng., IEEE, 2007: pp. 472–479. doi:10.1109/BIBE.2007.4375603.

[17] M. Hanselmann, M. Kirchner, B.Y. Renard, E.R. Amstalden, K. Glunde, R.M.A. Heeren, F.A. Hamprecht, Concise Representation of Mass Spectrometry Images by Probabilistic Latent Semantic Analysis, Anal. Chem. 80 (2008) 9649–9658. http://pubs.acs.org/doi/abs/10.1021/ac801303x.

[18] J. Yang, O. Rübel, M. Prabhat, M.W. Mahoney, B.P. Bowen, Identifying important ions and positions in mass spectrometry imaging data using CUR matrix decompositions, Anal. Chem. (2015) 150331082318005.

doi:10.1021/ac5040264.

[19] J.M. Fonville, C.L. Carter, L. Pizarro, R.T. Steven, A.D. Palmer, R.L. Griffiths, P.F. Lalor, J.C. Lindon, J.K. Nicholson, E. Holmes, J. Bunch, Hyperspectral Visualization of Mass Spectrometry Imaging Data, Anal. Chem. 85 (2013) 1415–1423. doi:10.1021/ac302330a.

[20] L.J.P. Van Der Maaten, G.E. Hinton, Visualizing high-dimensional data using t-sne, J. Mach. Learn. Res. 9 (2008) 2579–2605. doi:10.1007/s10479-011-0841-3.

[21] T. Alexandrov, M. Becker, S.-O. Deininger, G. Ernst, L. Wehder, M. Grasmair, F. von Eggeling, H. Thiele, P. Maass, Spatial Segmentation of Imaging Mass Spectrometry Data with Edge-Preserving Image Denoising and Clustering, J. Proteome Res. 9 (2010) 6535–6546. http://pubs.acs.org/doi/abs/10.1021/pr100734z.

[22] S.-O. Deininger, M.P. Ebert, A. Fütterer, M. Gerhard, C. Ro̧cken, MALDI Imaging Combined with Hierarchical Clustering as a New Tool for the Interpretation of Complex Human Cancers, J. Proteome Res. 7 (2008) 5230–5236. http://pubs.acs.org/doi/abs/10.1021/pr8005777.

[23] R. Van de Plas, J. Yang, J. Spraggins, R.M. Caprioli, Image fusion of mass spectrometry and microscopy: a multimodality paradigm for molecular tissue mapping, Nat. Methods. 12 (2015) 366–372. doi:10.1038/nmeth.3296.

[24] N. Verbeeck, J. Yang, B. De Moor, R.M. Caprioli, E. Waelkens, R. Van de Plas, Automated anatomical interpretation of ion distributions in tissue: linking imaging mass spectrometry to curated atlases., Anal. Chem. 86 (2014) 8974–8982. doi:10.1021/ac502838t.

[25] W.M. Abdelmoula, R.J. Carreira, R. Shyti, B. Balluff, R.J.M. van Zeijl, E.A. Tolner, B.F.P. Lelieveldt, A.M.J.M. van den Maagdenberg, L.A. McDonnell, J. Dijkstra, Automatic registration of mass spectrometry imaging data sets to the Allen brain atlas., Anal. Chem. 86 (2014) 3947–54. doi:10.1021/ac500148a.

[26] E.S. Lein, M.J. Hawrylycz, N. Ao, M. Ayres, A. Bensinger, A. Bernard, A.F. Boe, M.S. Boguski, K.S. Brockway, E.J. Byrnes, L. Chen, T.M. Chen, M.C. Chin, J. Chong, B.E. Crook, A. Czaplinska, C.N. Dang, S. Datta, N.R. Dee, A.L. Desaki, T. Desta, E. Diep, T.A. Dolbeare, M.J. Donelan, H.W. Dong, J.G. Dougherty, B.J. Duncan, A.J. Ebbert, G. Eichele, L.K. Estin, C. Faber, B.A. Facer, R. Fields,

S.R. Fischer, T.P. Fliss, C. Frensley, S.N. Gates, K.J. Glattfelder, K.R. Halverson, M.R. Hart, J.G. Hohmann, M.P. Howell, D.P. Jeung, R.A. Johnson, P.T. Karr, R. Kawal, J.M. Kidney, R.H. Knapik, C.L. Kuan, J.H. Lake, A.R. Laramee, K.D. Larsen, C. Lau, T.A. Lemon, A.J. Liang, Y. Liu, L.T. Luong, J. Michaels, J.J. Morgan, R.J. Morgan, M.T. Mortrud, N.F. Mosqueda, L.L. Ng, R. Ng, G.J. Orta, C.C. Overly, T.H. Pak, S.E. Parry, S.D. Pathak, O.C. Pearson, R.B. Puchalski, Z.L. Riley, H.R. Rockett, S.A. Rowland, J.J. Royall, M.J. Ruiz, N.R. Sarno, K. Schaffnit, N. V Shapovalova, T. Sivisay, C.R. Slaughterbeck, S.C. Smith, K.A. Smith, B.I. Smith, A.J. Sodt, N.N. Stewart, K.R. Stumpf, S.M. Sunkin, M. Sutram, A. Tam, C.D. Teemer, C. Thaller, C.L. Thompson, L.R. Varnam, A. Visel, R.M. Whitlock, P.E. Wohnoutka, C.K. Wolkey, V.Y. Wong, M. Wood, M.B. Yaylaoglu, R.C. Young, B.L. Youngstrom, X.F. Yuan, B. Zhang, T.A. Zwingman, A.R. Jones, Genome-wide atlas of gene expression in the adult mouse brain, Nature. 445 (2007) 168–176. doi:nature05453 [pii]₩r10.1038/nature05453.

[27] R.J. Carreira, R. Shyti, B. Balluff, W.M. Abdelmoula, S.H. Van Heiningen, R.J. Van Zeijl, J. Dijkstra, M.D. Ferrari, E.A. Tolner, L.A. McDonnell, A.M.J.M. Van

Den Maagdenberg, Large-scale mass spectrometry imaging investigation of consequences of cortical spreading depression in a transgenic mouse model of migraine, J. Am. Soc. Mass Spectrom. 26 (2015) 853–861. doi:10.1007/s13361-015-1136-8.

[28] K. Skraskova, A. Khmelinskii, W.M. Abdelmoula, S. De Munter, M. Baes, L. McDonnell, J. Dijkstra, R.M.A. Heeren, Precise anatomic localization of accumulated lipids in Mfp2 deficient murine brains through automated registration of SIMS images to the allen brain atlas, J. Am. Soc. Mass Spectrom. 26 (2015) 948–957. doi:10.1007/s13361-015-1146-6.

[29] R. Bakker, P. Tiesinga, R. Kötter, The Scalable Brain Atlas: Instant Web-Based Access to Public Brain Atlases and Related Content, Neuroinformatics. 13 (2015) 353–366. doi:10.1007/s12021-014-9258-x.

[30] E.A. Papp, T.B. Leergaard, E. Calabrese, G.A. Johnson, J.G. Bjaalie, Waxholm Space atlas of the Sprague Dawley rat brain., Neuroimage. 97 (2014) 374–86. doi:10.1016/j.neuroimage.2014.04.001.

[31] M. Sergejeva, E.A. Papp, R. Bakker, M.A. Gaudnek, Y. Okamura-Oho, J. Boline, J.G. Bjaalie, A. Hess, Anatomical landmarks for registration of

experimental image data to volumetric rodent brain atlasing templates, J. Neurosci. Methods. 240 (2015) 161–169. doi:10.1016/j.jneumeth.2014.11.005.

[32] L.J. Kjonigsen, S. Lillehaug, J.G. Bjaalie, M.P. Witter, T.B. Leergaard, Waxholm Space atlas of the rat brain hippocampal region: Three-dimensional delineations based on magnetic resonance and diffusion tensor imaging, Neuroimage. 108 (2015) 441–449. doi:10.1016/j.neuroimage.2014.12.080.

[33] J. Yang, R.M. Caprioli, Matrix sublimation/recrystallization for imaging proteins by mass spectrometry at high spatial resolution., Anal. Chem. 83 (2011) 5728–34. doi:10.1021/ac200998a.

[34] J.M. Spraggins, D.G. Rizzo, J.L. Moore, K.L. Rose, N.D. Hammer, E.P. Skaar, R.M. Caprioli, MALDI FTICR IMS of Intact Proteins: Using Mass Accuracy to Link Protein Images with Proteomics Data., J. Am. Soc. Mass Spectrom. 26 (2015) 974–85. doi:10.1007/s13361-015-1147-5.

[35] M. Hawrylycz, R.A. Baldock, A. Burger, T. Hashikawa, G.A. Johnson, M. Martone, L. Ng, C. Lau, S.D. Larsen, J. Nissanov, L. Puelles, S. Ruffins, F. Verbeek, I. Zaslavsky, J. Boline, Digital Atlasing and Standardization in the Mouse Brain, PLOS Comput. Biol. 7 (2011) e1001065.

http://www.ploscompbiol.org/article/info:doi/10.1371/journal.pcbi.1001065.

[36] International Neuroinformatics Coordinating Facility, INCF website, (2016). http://software.incf.org/software/waxholm-space-atlas-of-the-sprague-dawley-rat-brain/download (accessed February 9, 2016).

[37] D. Kroon, MATLAB Central File Exchange, Read Medical Data 3D, Read Med. Data 3D. (n.d.). http://nl.mathworks.com/matlabcentral/fileexchange/29344-read-medical-data-3d (accessed February 12, 2014).

[38] W.M. Abdelmoula, K. Škrášková, B. Balluff, R.J. Carreira, E.A. Tolner, B.P.F. Lelieveldt, L. van der Maaten, H. Morreau, A.M.J.M. van den Maagdenberg, R.M. a Heeren, L. a McDonnell, J. Dijkstra, Automatic generic registration of mass spectrometry imaging data to histology using nonlinear stochastic embedding., Anal. Chem. 86 (2014) 9204–11. doi:10.1021/ac502170f.

[39] J. Oetjen, M. Aichler, D. Trede, J. Strehlow, J. Berger, S. Heldmann, M. Becker, M. Gottschalk, J.H. Kobarg, S. Wirtz, S. Schiffler, H. Thiele, A. Walch, P. Maass, T. Alexandrov, MRI-compatible pipeline for three-dimensional MALDI imaging mass spectrometry using PAXgene fixation., J. Proteomics. 90 (2013) 52–60. doi:10.1016/j.jprot.2013.03.013.

[40] T.K. Sinha, S. Khatib-Shahidi, T.E. Yankeelov, K. Mapara, M. Ehtesham, D.S. Cornett, B.M. Dawant, R.M. Caprioli, J.C. Gore, Integrating spatially resolved three-dimensional MALDI IMS with in vivo magnetic resonance imaging., Nat. Methods. 5 (2008) 57–9. doi:10.1038/nmeth1147.

[41] A.S. Attia, K.A. Schroeder, E.H. Seeley, K.J. Wilson, N.D. Hammer, D.C. Colvin, M.L. Manier, J.J. Nicklay, K.L. Rose, J.C. Gore, R.M. Caprioli, E.P. Skaar, Monitoring the inflammatory response to infection through the integration of MALDI IMS and MRI., Cell Host Microbe. 11 (2012) 664–73. doi:10.1016/j.chom.2012.04.018.

[42] A. Myronenko, Non-rigid Image Registration: Regularization, Algorithms and Applications, Oregon Health & Science University, 2010. http://books.google.com/books?id=uS3pZwEACAAJ&dq=non+rigid+image+registration+regularization+inauthor:andriy+myronenko&hl=&cd=1&source=gbs_api.

[43] A. Myronenko, Medical Image Registration Toolbox - Andriy Myronenko, (2013). https://sites.google.com/site/myronenko/research/mirt (accessed October 7, 2013).

[44] M. Grant, S. Boyd, Graph implementations for nonsmooth convex programs BT - Recent Advances in Learning and Control, in: V. Blondel, S. Boyd, H. Kimura (Eds.), Recent Adv. Learn. Control, Springer-Verlag Limited, 2008: pp. 95–110. http://stanford.edu/~boyd/graph_dcp.html.

[45] M. Grant, S. Boyd, CVX: Matlab Software for Disciplined Convex Programming, version 2.0 beta, 2012. http://cvxr.com/cvx.

[46] I.T. Jolliffe, Principal Component Analysis, Second Edition, Springer, 2002. http://books.google.com/books?id=_olByCrhjwIC&printsec=frontcover&dq=intitle:Principal+Component+Analysis+Second+Edition+joliffe&hl=&cd=1&source=gbs_api.

[47] M. Dhenain, S.W. Ruffins, R.E. Jacobs, Three-Dimensional Digital Mouse Atlas Using High-Resolution MRI, Dev. Biol. 232 (2001) 458–470. doi:10.1006/dbio.2001.0189.